

High power ECRH and ECCD in moderately collisional ASDEX Upgrade H-modes and status of EC system upgrade

J. Stober^{1,a}, F. Sommer¹, C. Angioni¹, A. Bock¹, E. Fable¹, F. Leuterer¹, F. Monaco¹, S. Müller¹, M. Münich¹, B. Petzold¹, E. Poli¹, M. Schubert¹, H. Schütz¹, D. Wagner¹, H. Zohm¹, the ASDEX Upgrade Team¹, W. Kasperek², B. Plaum², A. Meier³, Th. Scherer³, D. Strauß³, J. Jelonek³, M. Thumm³, A. Litvak⁴, G.G. Denisov⁴, A.V. Chirkov⁴, E.M. Tai⁵, L.G. Popov⁵, V.O. Nichiporenko⁵, V.E. Myasnikov⁵, E.A. Soluyanov⁵, and V. Malygin⁵

¹Max-Planck-Institut für Plasmaphysik, Garching, Germany

²Institut für Grenzflächenverfahrenstechnik und Plasmatechnologie, Universität Stuttgart, Stuttgart, Germany

³Karlsruhe Institute of Technology, Karlsruhe, Germany

⁴Institute of Applied Physics, RAS, Nizhny Novgorod, Russia

⁵GYCOM Ltd., Nizhny Novgorod and Moscow, Russia

Abstract. This contribution deals with H-modes with significant heat exchange between electrons and ions, but which can still show large differences between electron and ion-temperatures especially inside half minor radius. These conditions are referred to as moderately collisional. A systematic study shows that an increasing fraction of electron heating increases the transport in the ion channel mainly due to the dependence of the ITG dominated ion transport on the ratio T_e/T_i in agreement with modeling. The rotational shear in the plasmas under study was so small that it hardly influences ITG stability, such that variations of the rotation profile due to a change of the heating method were of minor importance. These findings connect to studies of advanced tokamak scenarios using ECCD as a tool to modify the q-profile. The electron heating connected to the ECCD tends to increase the transport in the ion channel quite in contrast to the goal to operate at reduced current but with increased confinement. The confinement only increases as the fraction of ion heating is increased by adding more NBI. An ITER case was modeled as well. Due to the larger value of $\nu_{ei} \cdot \tau_E$ the ratio T_e/T_i is only moderately reduced even with strong electron heating and the confinement reduction is small even for the hypothetical case of using only ECRH as additional heating. Finally the paper discusses the ongoing upgrade of the AUG ECRH-system.

1 Introduction

During the last years the ECRH system on ASDEX Upgrade (AUG) has been extended by 4 units delivering 1 MW at 140 GHz for 10 s each (for the experiments described here only 3 out of 4 were available). The new units are capable of 2-frequency operation (2nd frequency 105 GHz) and the new launchers can be rotated fast around one axis during a discharge for the purpose of MHD-control [1]. One of the units will be extended with two additional intermediate frequencies as soon as the corresponding vacuum-window issues are solved [2]. Additionally the initial ECRH system with 4 units with 0.5 MW / 2 s pulses at 140 GHz is still available. With 3 new units and 4 initial units close to 4 MW of ECRH with 140 GHz can be delivered to the plasma which is among the top levels reached world wide so far. This high power was used to systematically compare the heating of H-modes with ECRH and NBI. In Section 2 the results are described. A major finding is the increase of transport in the ion channel due to increased ITG-turbulence. The latter in-

creases due to an increasing ratio of T_e/T_i . This finding has important consequences especially for scenarios which use ECCD to modify the q-profile on a large radial scale, since ECCD works most efficiently at low collisionality, i.e. where T_e/T_i changes strongly if the fraction of electron and ion heating is changed. This can lead to a significant loss of performance if ECCD is added to such plasmas. Experimental and modeling results are discussed in section 3. Section 4 discusses the effect on ITER. In ITER a difference between T_e and T_i is more effectively counteracted by the heat exchange given the larger volume. Therefore even full additional heating by ECRH only may not significantly effect the central ion temperature and Q . In the final section 5 a further upgrade of the EC system on AUG is discussed replacing the initial units by four more 1 MW / 10 s units using the old launching positions. Status of the construction work and the actual time schedule are discussed.

^ae-mail: Joerg.Stober@ipp.mpg.de

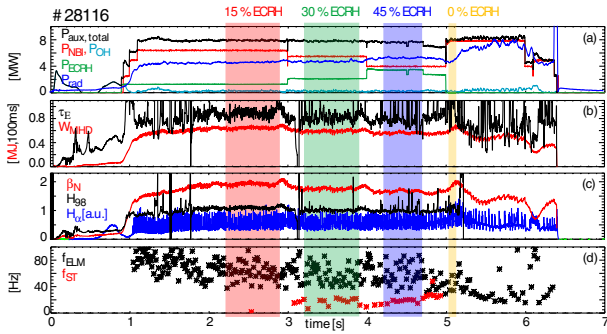


Figure 1. Overview plot of a high power, moderately collisional discharge: Plot (a): total auxiliary (black), NBI (red), central ECRH (green), Ohmic (light blue) and radiated power (blue); plot (b): stored energy W_{MHD} (red), and energy confinement time τ_E (black); plot (c): normalised beta β_N (red), confinement factor H_{98} (black) and H_α radiation in the divertor (blue); plot (d): ELM (black) and sawtooth frequency (red).

2 Systematic variation of the fraction of electron heating

The effect of the heating mix on the transport in the electron and ion channel has already been addressed in the EC17 meeting [1]. Those results are discussed in more detail in [3]. In summary, replacing NBI by central ECRH leads to a significant drop of the ion temperature while T_e increases only marginally, leading to the hypothesis that small changes in the ratio T_e/T_i effect the critical gradient for the dominant ITG mode as already shown in [4] for $T_i \geq T_e$. The initial experiments [3] were done at low input power ($1.25 \times$ the L/H-threshold power) in order to be able to reach 100% of ECR heating resulting also in a significant gas flux in order to prevent W accumulation at too low density. As a consequence the collisionality and the heat exchange between electrons and ions was rather high. Although this is a situation also found in ITER it makes the separation of the transport in both channels difficult and the experiments were repeated with 8 MW instead of 3 MW. In this case up to 45% of the heating power were supplied by ECRH. In order to check if the underlying physics is included in actual parameter-free models, the toroidal-gyro-Landau-fluid code TGLF [5, 6] has been used for both cases. This work is described in detail in [7–9]. Here a case with high heating power and correspondingly lower collisionality is discussed in order to convince the reader that TGLF describes well the observed behaviour. Figure 1 shows time traces of the discharge probing several ratios of the power mix keeping the total power constant. For three ratios (15%, 30% and 45%) steady phases were achieved marked with coloured vertical bars. For the NBI only case no steady phase was achieved due to central tungsten accumulation leading to the rise in radiation and the drop in stored energy. This phenomenon is generally observed for H-modes in ASDEX Upgrade below a certain level of gas-puff after the original graphite tiles were coated with W [10]. The NBI only phase is therefore disregarded in the following. Figure 2 shows the

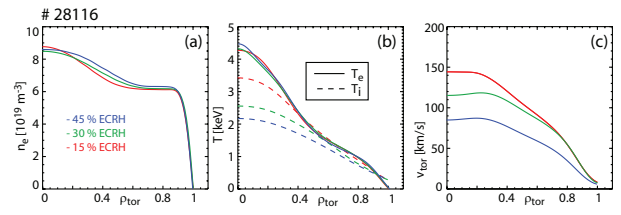


Figure 2. Averaged kinetic profiles of the high power, low collisionality discharge during different heating phases (red: 15% ECRH, green: 30% ECRH, blue: 45% ECRH): plot (a): electron density; plot (b): electron (solid) and ion (dashed) temperature; plot (c): toroidal rotation.

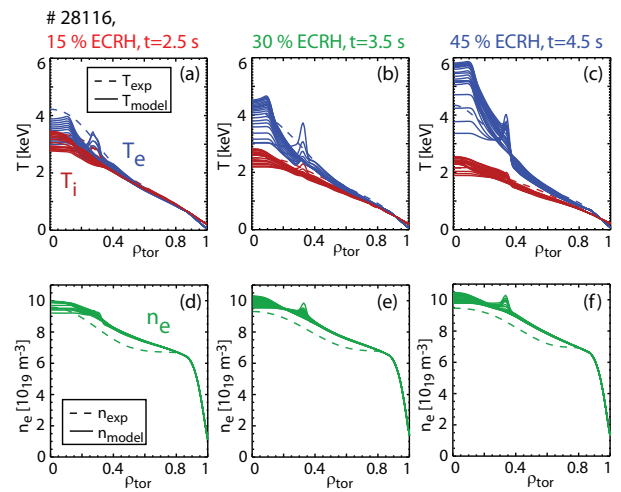


Figure 3. Combined temperature and density modeling by TGLF of the high power, low collisionality discharge. Plot (a) to (c): comparison of T_e (blue) and T_i (red) with the experimental profiles. The time averaged experimental profiles are shown as dashed lines, the modeled profiles as solid lines. Plot (d) to (f): electron temperature modeling.

kinetic profiles of the three steady phases with the same colour code as the vertical bars in figure 1. The reduction of T_i in the inner half of the plasma with increasing EC fraction is obvious and more pronounced than in the case with higher collisionality. In both cases the electron temperature is hardly changed. The change in rotation is also significant, but the corresponding rotational shear is low as compared to the ITG growth rates calculated with the gyrokinetic code GS2 [11, 12]. Therefore the variation in rotation is not considered very important here. We note that this was different for earlier experiments with high rotational shear and $T_e < T_i$ as described in [4]. The modeling of the behaviour was attempted with the TGLF code in the ASTRA/SPIDER framework [13] and rather convincing results were achieved for both levels of collisionality. The results for the low collisionality case corresponding to figures 1,2 is shown in figure 3. Electron density and ion temperature are very well reproduced. The electron temperature is predicted to increase in average in contrast to experiment. The figure shows several curves for the modeled T_e . This variation is caused by the im-

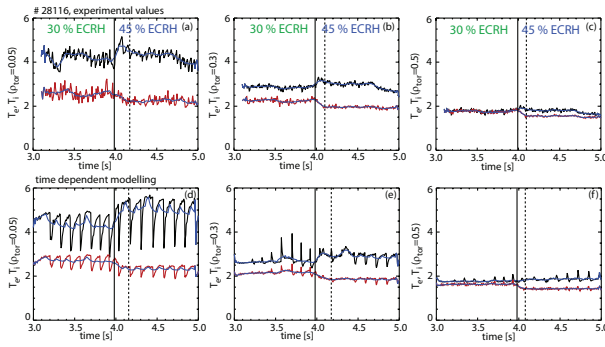


Figure 4. Time dependent modeling of the electron and ion temperatures when switching the heating mix. Plot (a)-(c): experimental evolution, plot (d)-(f): modeled evolution. Shown are the center ($\rho_r=0.05$), between inversion and mixing radius ($\rho_r=0.3$) and mid radius ($\rho_r=0.5$). Note that at 4.7 s some ECRH power was lost leading to the drop in the experimental T_e data afterwards. This drop of power was not included into the modeling.

plemented sawtooth model which has been added in AS-TRA. The Kadomtsev-type model has been adjusted such that it predicts the inversion radius correctly. With these settings it underestimates the sawtooth frequency for the cases studied here. The mismatch of the frequency and the correspondingly larger sawteeth may be one reason for the slight mismatch in T_e of experiment and model. Figure 3 analyses temporal averages of the experimental data corresponding to the coloured vertical bars in figure 1 neglecting temporal variations leading to the striking experimental result that an increase of the electron heating keeps T_e constant but lowers T_i . More insight can be gained by looking into the temporal behaviour. Figure 4 shows experimental and modeled time traces for the transition period from 30% to 45% of EC heating (transition from the green to the blue bar in figure 1). T_e, T_i values at $\rho_r = 0.05, 0.3$ and 0.5 are shown. Again the discrepancy of sawteeth frequency and amplitude is obvious in the plasma center. Apart from this the agreement is quite good considering that the model does not contain any tuning parameters. Also the time constant of the transition indicated by the vertical dashed bar is reproduced well. We see that also in the experiment the T_e values tend to rise initially as the electron heating is increased but drop again as T_i reduces in contrast to the model. As mentioned above it cannot be decided here if this is due to the sawtooth mismatch or to an insufficiency of the TGLF model. In any case the TGLF modeling supports the initial assumption that an increasing ratio of T_e/T_i enforces ITG-turbulence thereby increasing radial transport especially in the ion channel. On the basis of this good agreement TGLF can be used for predictive purposes as described in the following sections. We note here that although the modelling is parameter-free, the boundary condition is defined at the pedestal top, i.e. $\rho_r = 0.85$. This means that no model for the H-mode pedestal is included and any prediction cannot be better than the estimate of the pedestal parameters. Note that for the results shown in figures 3,4 this is not an issue since the boundary

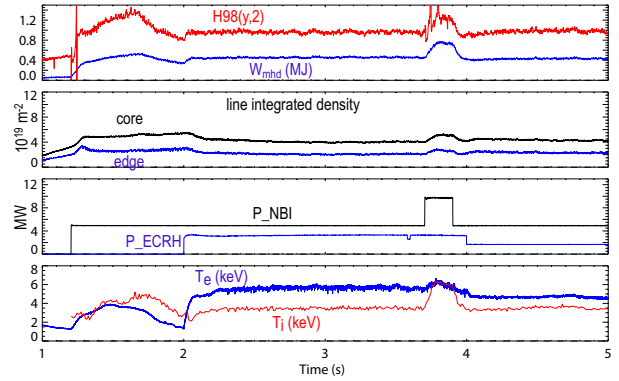


Figure 5. H-mode discharge (#27351) with ctr-ECCD inside $\rho_r < 0.4$ with $q_{min} > 1$, $I_p = 0.8$ MA, $B_t = -2.5$ T. Note the variation of T_e, T_i, W_{mhd} and H-factor as the ECRH sets in and as the NBI power is doubled. The roll-over of W_{mhd} and the temperatures around 1.5 s is due to W accumulation which is caused by a lack of central electron heating during the NBI-only phase.

conditions on the pedestal top are given in this case by the dedicated edge and pedestal diagnostics on AUG.

3 Consequences for AT scenario development

As already discussed in the previous section, the detrimental effect of the electron heating on the transport in the ion channel is more pronounced for the case with lower collisionality since the reduced electron-ion heat-exchange allows a larger difference between T_e and T_i and thus a larger ratio T_e/T_i which reduces the critical R/L_{Ti} for the ITG-onset. This is at least true for experiments within machines of similar size. In larger machines T_e/T_i may be smaller even at lower collisionality since the improved thermal insulation forces a better equilibration. This will be discussed in the next section.

Here we consider effects on the study of advanced scenarios in today's medium size machines such as AUG, trying to use ECCD most efficiently for current profile modifications to test the effect of such variations on confinement and maximum achievable β -values. The efficiency of current drive is highest for the lowest collisionality. Thus such scenarios are most prone to an increase of the ion transport by electron heating, which is inevitably connected to ECCD. Figure 5 shows attempts on AUG to increase the minimum q -value by a broad profile of ctr-ECCD inside $\rho_r < 0.4$. The discharge can be separated into three phases. First there is an NBI-only phase (5 MW). During this phase both temperatures rise initially and an H-factor above 1.2 is reached transiently. The reduction of the central temperatures and the stored energy is due to W accumulation as already discussed in the previous section. The W accumulation is removed by the central electron heating connected with the ctr-ECCD. Although the heating power is increased by 70% ($P_{ECCD} \approx 3.5$ MW) the stored energy does not reach its maximum value in the NBI-only phase. Correspondingly the H-factor is low

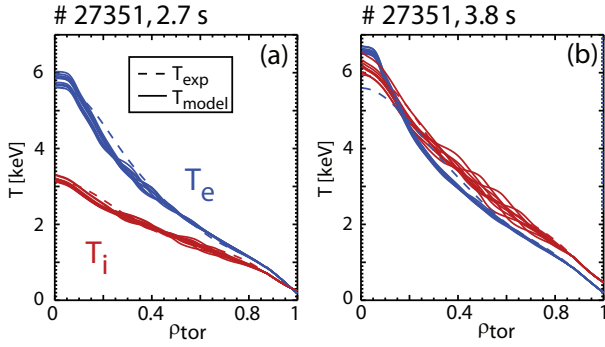


Figure 6. TGLF modeling for two phases of discharge #27351 (see fig. 5). Plot (a): 3.2 MW ECRH and 5 MW NBI power. The dashed curves show the averaged experimental profiles, while the solid curves show the modeled data (T_e : blue, T_i : red). Plot (b): 3.2 MW ECRH and 10 MW NBI power.

(0.85). From the discussion above we assume that this poor confinement is due to an increase of the ion transport driven by the large value of T_e/T_i . In the third phase the NBI heating is increased by another 5 MW. Under these conditions (E_{beam} 60 keV and 93 keV) NBI dominantly heats the ions. Indeed in this phase T_i increases up to T_e , while the latter is hardly changed and the H-factor reaches 1.2 again. Figure 6 shows the result of the TGLF modeling [7–9], here without a sawtooth model, since the ctr-ECCD has removed the $q=1$ surface from the plasma. We note the excellent prediction of the peaking of the temperature profiles. For the future of the AT programme at AUG, TGLF modeling seems to be an appropriate tool to predict the effect of the ECCD on the ion temperature already in the planning phase and to add sufficient NBI heating to keep the ion temperature close to the electron temperature as it should be the case for a reactor relevant scenario. Experiments along this route are still planned for the 2014 campaign. Unfortunately these low collisionality H-modes cannot easily be combined with SOL radiation-cooling using N_2 seeding as usually done at AUG to protect the divertor tiles for high levels of heating power. In that sense the high level of NBI power which has to be added to the ECCD may turn out to limit the discharge length.

4 Consequences for ITER

As mentioned already in the previous section for larger machines T_e/T_i is expected to be closer to unity as compared to smaller machines with the same collisionality and heating mix. The reason being that the thermal insulation (τ_E) increases such that the radial heat flux decreases relative to the heat exchange fluxes. A dimensionless quantity characterising this behaviour is the product of $\tau_E \cdot \nu_{ei}$ (the latter to be taken as an average or at a fixed radius)¹.

¹One may want to normalize this product with the ratio m_e/m_i , since the heat exchange is given by electron-ion collisions whereas neoclassical heat transport is dominated by ion-ion collisions, but since we do not make any quantitative statements here, this is not relevant.

For example, the discharge discussed in the previous section has a collisionality close to ITER but a much lower confinement time. Therefore in ITER similarly good conditions for ECCD can be expected with significantly less separation of T_e and T_i .

In principle this separation of T_e, T_i in ITER can be predicted using TGLF modeling and assumptions for pedestal values of temperature and density. As a start this has been done for the ITER baseline Q=10 scenario. For the boundary values and heating powers we use values from [14]. We apply exactly the same modeling procedure and tools as used in this work for ASDEX Upgrade plasmas. ITER Q=10 operation foresees a magnetic field of 5.3 T, a plasma current of 15 MA, and includes substantial α -heating from the fusion reaction of deuterium with tritium. The poloidal plasma equilibrium was as well taken from reference [14] for the ITER baseline inductive scenario (figure 7 (a), red). The shape is similar to the equilibrium of ASDEX Upgrade, with a higher elongation and triangularity, but enlarged by a factor of 3 (blue). The profiles for temperatures and densities from [14] are shown as dashed lines in figure 7 (plots (b-d)). These are obtained from a model based on gyro-bohm scaling laws and profile consistency [15]. The boundary values for the TGLF calculation have been taken at $\rho_t = 0.85$. The small difference between the T_e and T_i becomes apparent over the entire plasma radius. The edge density profile has a pedestal top value of around $10 \cdot 10^{19} \text{ 1/m}^3$, corresponding to 85 % of the Greenwald density (plot (c), green lines). As in [14] we assume a 50:50 mix of deuterium and tritium (in our modeling described by one ion species with mass $A = 2.5$), an expected concentration of Helium of 4%, and a radially independent $Z_{eff} = 1.8$. This requires an additional impurity species, and we choose carbon with a concentration of 2.4 %. The two impurities are realised by one species with concentration weighted mass and charge which is used as a second kinetic ion species in TGLF. The integrated auxiliary heating power is given as 40 MW during the burn phase in [14]. We chose a centrally peaked Gaussian heating profile which reaches half its maximum value at $0.45\rho_t$. The power is equally distributed between electrons and ions. In addition we assume that 20 MW are radiated away by the electrons, almost exclusively due to bremsstrahlung and cyclotron radiation (in [14] this number is 27 MW). The radiation has the same profile as the heat deposition to the electrons by external heating. Due to the ideal topology of flux surfaces in the core, TGLF shows stable micro-instabilities leading to a predicted transport approaching zero. However, in reality a number of core MHD activities exists, which lead to a flattening of the kinetic profiles and cannot be described by the code in the framework of this investigation. This is handled by the application of an artificial diffusivity of $0.25 \text{ m}^2/\text{s}$ in the core of the plasma up to $\rho_t \leq 0.2$. The results of the modeling (solid lines) are compared with the profiles from [14] (dashed) in figure 7. In plot (b) the electron (blue) and ion (red) temperatures are shown. The electron temperature is higher by 15 % compared to the ion temperature. Due to the large size of

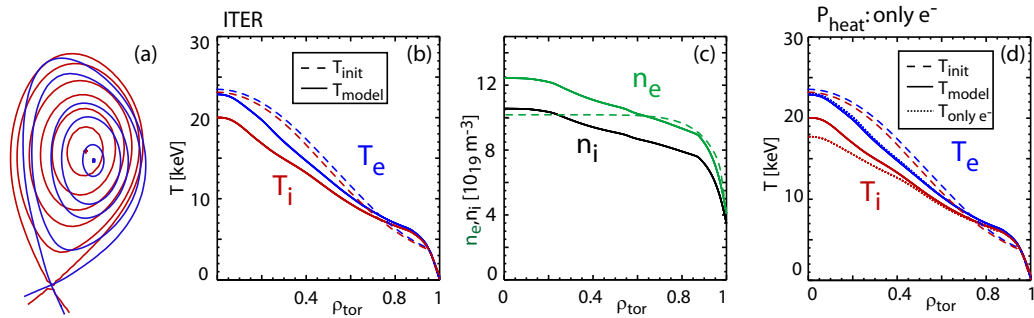


Figure 7. Plot (a): comparison of ITER equilibrium (blue) with typical equilibrium of ASDEX Upgrade used in the experiments for this work scaled by a factor of 3 (red). ITER modeling with TGLF (solid lines) in comparison with the profiles taken from reference [14](dashed) used as boundary condition at $\rho_t = 0.85$. Plot (b): Modeling of the electron (blue) and ion (red) temperature. Plot (c): Modeling of the electron (green) and ion (black) density. Plot (d): Modeling with external electron heating only.

the device, this difference is still small despite the fact that only 25 % of the α -power is going to the ions. The modeled electron density profile (plot (c)) shows a peaking of $n_0/\langle n \rangle_V = 1.3$. Motivated by recent results obtained at JET [16] we tested the evolution of the profiles when the modeling is initialised with hollow starting profiles. Also in these cases the density converges to the same peaking of 1.3. The reversal from the initial hollowness (peaking = 0.9) to a slight peaking happens very fast within only 0.5 s, the equilibration to a steady state peaked profile takes roughly 10 s. In the same plot the total ion density profile is shown in black, which has values of 15 % below the electron density. The dilution of the density by the small impurity content of 4 % Helium and 2.4 % Carbon is evident. The normalised gradients averaged between $\rho_t = 0.4$ and $\rho_t = 0.7$ are $R/L_{Te} = 5.4$, $R/L_{Ti} = 5.0$ and $R/L_{ne} = 1.3$.

The presented configuration leads to a total fusion power of 460 MW, from which 368 MW are lost from the plasma by 14 MeV neutrons. The remaining 92 MW are carried by fast α -particles. They transfer 68 MW to the electrons and 24 MW to the ions. The result is a predominantly electron heated plasma, also taking into account the external heating, which is expected to heat both species equally. This leads to a value of $Q = 11.5$, which is close to the envisaged value of 10 in the D-T phase of ITER [14], i.e. in our simulation the peaking of the density profile over-compensates the reduction of the fusion rate due to the reduced ion temperature.

The sensitivity of the modeling results was analysed with respect to changes of the radiation and input power. Previously the assumption was made that all external heat deposited into the electrons is radiated away. Assuming no radiation, the modeled temperatures are basically unchanged and the fusion power increases by only 2.5 %. When assuming a doubling of P_{rad} , then $T_{e,c}$ decreases by 7 %, while $T_{i,c}$ is hardly changed and the fusion power decreases by only 4 %. Essentially less radiation means more electron heating which also in ITER slightly effects T_e/T_i decreasing the effect of the additional electron heating on ion temperature.

The other variation features a 50 % increase of the heating leading to $Q = 8$. We see that the value of Q cannot be deduced precisely only from heat demand considerations, since the kinetic profiles and the fusion power are not very sensitive to the amount of external heating power during the flat top phase. The required maximum injected external power depends more on the access of the H-mode during start up and the needed current drive for different scenarios [17, 18] and the latter may be a more crucial constraint for the determination of Q .

The previous assumption of 50:50 electron and ion heating was based on the mixed usage of NBI and ECRH. Assuming only ECRH, we performed the same modeling but putting all 40 MW of power into the electrons (with the same radial distribution as above) and no power into the ions. The modeled density profile is exactly the same. While T_e does not change, T_i decreases in the centre by 2 keV. Both temperatures are shown in figure 7 (d) as dotted lines in comparison with the previous modeling (solid lines) and the results from [14] (dashed lines). As a result, the total fusion power decreases by 6 %. We see that the change of heated species has a far greater influence on kinetic profiles in present medium size devices compared to future machines. The performance of the steady state burn phase in the ITER standard scenario decreases only slightly, when the external heating power is transferred solely to the electrons, e.g. by the use of ECRH. For operation at lower $\tau_E \cdot \nu_{ei}$ as will be the case for operation at lower current, Hydrogen-operation and steady-state scenarios effects of dominant electron heating may become relevant also in ITER. Details should be analysed similarly as presented here for the $Q=10$ burning phase.

We also analysed dependence of the discharge performance on the pedestal temperatures by reducing the boundary conditions of T_e and T_i by 10 % and 20 % individually. A 10 % decrease of the edge values leads to an 8 % decrease of the central T_e and 6 % of the central T_i . The fusion power is reduced by 15 %. This leads to a reduction of Q by 17 % to $Q = 9.5$. For a 20 % decrease of the edge temperatures the effects on the core temperatures and the fusion power double, reducing Q to 7.9. These

considerations confirm former studies (e.g. [19]) that the performance of future fusion devices crucially depends in 0th order on the pedestal top values of the temperatures and only in higher order on the heated species.

5 Motivation, status and time-schedule of the next ECRH-upgrade on AUG

In the introduction it has been pointed out that the physics results presented in this contribution heavily build on the extension of the ECRH system on AUG by a completely new system of four units capable of 105/140 GHz, 1 MW, 10 s each (ECRH 2). Since 2014 all four new units are used for routine operation. This new system proved to be a versatile tool for many physics studies and is used in the vast majority of AUG discharges, thereby creating an increasing demand on more ECRH power and reliability. Driven by the plan to study advanced tokamak scenarios with central ctr-ECCD, IPP decided in 2011 to finance another ECRH system (ECRH3) again with 4 units with 105/140 GHz, 1 MW, 10 s each, i.e. quite similar to ECRH2. The idea is to stay mainly with the approved technology. Major technological upgrades are the use of cryogen-free magnets, semiconductor-based body modulators and DC-cathode heaters. Unfortunately major parts of the electronics have to be redesigned due to short life-cycles of components. Together with the new system the high-power HV-supply will be extended re-using power supplies from the old HERA-storage ring at DESY. The launchers will be those of ECRH 1 (which will be definitely decommissioned) with some adaptations to the microwave optics and mechanics, but for the time being they will not be significantly upgraded with respect to the maximum applicable torque. This means that only movements with a few degrees per second will be possible during a discharge.

Building modifications were completed in 2013. The cooling system is almost ready approaching its first leakage test. Gyrotron sockets and MOU-frames are ready. Electronics construction and cabling is in process as is the production of quasi-optical components (mainly IPP work shops). The HV-cabinet is being equipped. The series modulators are IPP-built. The support for the transmission line is almost ready and the 87mm corrugated HE₁₁-mode wave-guides are being delivered. The major components have all been ordered. The body modulator and the cryomagnets will be tested in autumn 2014. Acceptance of the first gyrotron is planned a year later and a completion of the system is foreseen in 2017, according to the actual planning.

Acknowledgment

This project has received funding from the Euratom research and training programme 2014-2018.

References

[1] J. Stober, A. Bock, H. Höhnle, M. Reich, F. Sommer, W. Treutterer, D. Wagner, L. Gianone, A. Herrmann,

- F. Leuterer et al., EPJ Web of Conferences **32**, 02011 (2012)
- [2] G. Denisov et al., *Development in Russia of Gyrotrons for Fusion. Status and New Trends*. (2014), these conference proceedings
- [3] F. Sommer, J. Stober, C. Angioni, M. Bernert, A. Burckhart, V. Bobkov, R. Fischer, C. Fuchs, R. McDermott, W. Suttrop et al., Nuclear Fusion **52**, 114018 (2012)
- [4] A. Manini, C. Angioni, A.G. Peeters, F. Ryter, A. Jacchia, C.F. Maggi, W. Suttrop, ASDEX Upgrade Team, Nuclear Fusion **46**, 1047 (2006)
- [5] G. Staebler, J. Kinsey, R. Waltz, Physics of Plasmas **12**, 102508 (24) (2005)
- [6] J.E. Kinsey, G.M. Staebler, R.E. Waltz, Physics of Plasmas **15**, 055908 (2008)
- [7] F. Sommer, Phd thesis, LMU München (2013), also IPP report 1/352, <http://edoc.mpg.de/get.ep1?fid=114269&did=670413&ver=0>
- [8] F. Sommer, J. Stober, C. Angioni, E. Fable, M. Bernert, A. Burckhart, V. Bobkov, R. Fischer, C. Fuchs, R.M. McDermott et al., AIP Conference Proceedings **1580**, 153 (2014)
- [9] F. Sommer, J. Stober, C. Angioni, E. Fable et al., Nuclear Fusion (2014), submitted
- [10] O. Gruber, A.C.C. Sips, R. Dux, T. Eich, J.C. Fuchs, A. Herrmann, A. Kallenbach, C.F. Maggi, R. Neu, T. Pütterich et al., Nuclear Fusion **49**, 115014 (2009)
- [11] M. Kotschenreuther, G. Rewoldt, W. Tang, Computer Physics Communications **88**, 128 (1995)
- [12] W. Dorland, F. Jenko, M. Kotschenreuther, B.N. Rogers, Physical Review Letters **85**, 5579 (2000)
- [13] E. Fable, C. Angioni, A.A. Ivanov, K. Lackner, O. Maj, S.Y. Medvedev, G. Pautasso, G.V. Pereverzev, W. Treutterer, ASDEX Upgrade Team, Plasma Physics and Controlled Fusion **55**, 074007 (2013)
- [14] T. Casper, Y. Gribov, A. Kavin, V. Lukash, R. Khayrutdinov, H. Fujieda, C. Kessel, I. Organization, I.D. Agencies, Nuclear Fusion **54**, 013005 (2014)
- [15] W. Tang, Nucl. Fusion **26**, 1605 (2001)
- [16] A. Loarte, M. Leyland, J. Mier, M. Beurskens, I. Nunes, V. Parail, P. Lomas, G. Saibene, R. Sartori, L. Frassinetti et al., Nuclear Fusion **53**, 083031 (2013)
- [17] I. Chapman, J. Graves, O. Sauter, C. Zucca, O. Asunta, R. Buttery, S. Coda, T. Goodman, V. Igochine, T. Johnson et al., Nuclear Fusion **53**, 066001 (2013)
- [18] F. Poli, C. Kessel, P. Bonoli, D. Batchelor, B. Harvey, 55th Annual Meeting of the APS Division of Plasma Physics **58**, PO4 (2013)
- [19] J. Kinsey, G. Staebler, J. Candy, R. Waltz, R. Budny, Nuclear Fusion **51**, 083001 (2011)